POLITECNICO DI TORINO
Repository ISTITUZIONALE

Resonance condition and field distribution in line-defect photonic crystal cavities

Original
Resonance condition and field distribution in line-defect photonic crystal cavities / Saldutti, Marco; Mørk, Jesper; Gioannini, Mariangela. - PROCEEDINGS VOLUME 11301:(2020), p. 30. (Intervento presentato al convegno Novel In-Plane Semiconductor Lasers XIX, SPIE OPTO, 2020, San Francisco, California, United States tenutosi a San Francisco, California, United States) [10.1117/12.2545149].

Availability:
This version is available at: 11583/2798792 since: 2020-02-28T12:12:43Z

Publisher:
Society of Photo-Optical Instrumentation Engineers

Published
DOI:10.1117/12.2545149

Terms of use:

This article is made available under terms and conditions as specified in the corresponding bibliographic description in the repository

Publisher copyright
SPIE postprint/Author's Accepted Manuscript e/o postprint versione editoriale/Version of Record con

Copyright 2020 Society of PhotoOptical Instrumentation Engineers (SPIE). One print or electronic copy may be made for personal use only. Systematic reproduction and distribution, duplication of any material in this publication for a fee or for commercial purposes, and modification of the contents of the publication are prohibited.

(Article begins on next page)

16 April 2024

Resonance condition and field distribution in line-defect photonic crystal cavities

Marco Saldutti[a], Jesper Mørk[b], and Mariangela Gioannini[a]

[a]Politecnico di Torino, Corso Duca degli Abruzzi 24, IT-10129 Torino, Italy
[b]DTU Fotonik, Technical University of Denmark, Ørsteds Plads, DK-2800 Kgs. Lyngby, Denmark

ABSTRACT

By applying a recently proposed coupled-Bloch-mode approach, we have derived the resonance condition for the longitudinal modes of passive photonic crystal (PhC) line-defect cavities. We have derived simple expressions for the electric field depending on the size of the cavity and the order of the resonant mode. We have shown that, as the cavity becomes longer, the fundamental mode turns from FP-like to DFB-like and the fraction of its wavevector components within the light cone is gradually suppressed. Importantly, we have clarified the physical origin for this behaviour.

Keywords: Photonic crystal (PhC), photonic crystal cavities, Bloch modes, FP-like, DFB-like, radiation loss, Q-factor, coupled-mode theory

1. INTRODUCTION

Photonic crystal (PhC) lasers are promising candidates for on-chip and chip-to-chip light sources, as the cavity length can be scaled down to few micrometers while maintaining the quality-factor (Q-factor) high.[1] This allows PhC lasers to have low threshold current and small energy cost, with record values being recently reported.[2] PhC lasers can be integrated on silicon[3] and offer additional interesting functionalities, such as ultrafast frequency modulation,[4] self-sustained ultrashort pulse generation[5] and increased stability against external optical feedback.[6]

To maximize the Q-factor of a PhC cavity, the radiation loss must be kept as low as possible. At a given frequency, the time-averaged power radiated out of the cavity is proportional to the integral within the light cone of the spatial Fourier transform of the electric field intensity.[7] Therefore, suppressing the wavevector components of the field in the light cone is an effective strategy to maximize the Q-factor.[8] Research works based on finite-difference-time-domain (FDTD) simulations have distinguished the longitudinal modes of a passive PhC line-defect cavity into FP-like or DFB-like depending on the size of the cavity size and the order of the resonant mode.[9] The particular nature of the mode has been also correlated with the fraction of wavevector field components within the light cone, thus providing useful insights on the scaling of the Q-factor. However, a more fundamental understanding of this classification is missing.

In this work, we employ a recently proposed coupled-Bloch-mode approach[10] to analyze the resonance condition and electric field distribution in passive PhC line-defect cavities. We show that this approach provides the simple expressions suggested in[9] and clarifies the physical origin of the classification contained therein. Furthermore, we compute the relative fraction of the electric field intensity within the light cone for the fundamental mode and show that the scaling with the size of the cavity is in agreeement with other results reported in the literature.[11]

This paper is organized as follows: in Section 2, we briefly summarize the coupled-Bloch-mode approach and derive the resonance condition for a passive PhC line-defect cavity. In Section 3, we discuss the expansion of the Bloch modes of the cavity in a Fourier series, which is a key point to explain the FP-like or DFB-like nature of a resonant mode. In Section 4, we derive the real-space distribution of the electric field within the cavity for a generic resonant mode. In Section 5, we focus on the fundamental mode and analyze its real- and wavevector-space distribution. In Section 6, we finally draw the conclusions.

Further author information: (Send correspondence to M.S.)
M.S.: E-mail: marco.saldutti@polito.it

2. RESONANCE CONDITION

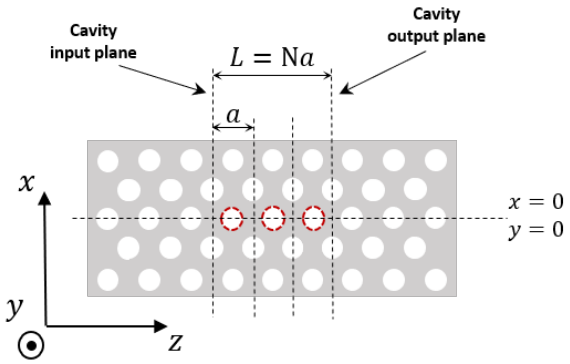

Figure 1: A LN PhC cavity with N = 3. The reference system and the choice of the unit cell adopted in this paper are shown. With this choice, a LN cavity is modelled as made up of N unit cells.

A so called LN cavity is obtained by omitting N holes in a PhC slab.[9] As an example, Fig. (1) shows the top view of a L3 cavity (the holes encircled by red are intented to be removed) together with the reference system adopted in this paper. In,[10] the coupled-Bloch-mode (CBM) approach has been applied to the analysis of various PhC cavities based on line-defect waveguides (LDWGs). The electric field in a LDWG with a complex refractive index perturbation is expanded on the forward- (+) and backward-propagating (-) Bloch modes

$$\mathbf{E}(\mathbf{r},\omega) = \psi_+(z,\omega)\mathbf{e}_0^+(\mathbf{r},\omega)e^{+ik_z(\omega)z} + \psi_-(z,\omega)\mathbf{e}_0^-(\mathbf{r},\omega)e^{-ik_z(\omega)z} \tag{2.1}$$

Here, $\mathbf{e}_0^\pm$ are periodic along z with the period given by the PhC lattice constant a and $\psi_\pm(z,\omega)$ are slowly-varying envelopes which account for gain and refractive index perturbations. The wavevector k_z is taken in the left around of the *second* Brillouin zone (BZ) ($k_z \in [\pi/a, 2\pi/a]$), where its derivative with respect to frequency is positive and the corresponding Bloch mode is thus forward-propagating. The slowly-varying envelopes are governed by the CBM equations

$$\begin{aligned} \partial_z\psi_+ &\simeq i\kappa_{11,q=0}(\omega)\psi_+ + i\kappa_{12,q=1}(\omega)e^{+2i\delta(\omega)z}\psi_- \\ -\partial_z\psi_- &\simeq i\kappa_{21,q=-1}(\omega)e^{-2i\delta(\omega)z}\psi_+ + i\kappa_{11,q=0}(\omega)\psi_- \end{aligned} \tag{2.2}$$

where $\delta(\omega) = \pi/a - k_z(\omega)$ is the detuning from the band edge, $\kappa_{11,q=0}(\omega)$ is the self-coupling coefficient and $\kappa_{12,q=1;21,q=-1}(\omega)$ are the cross-coupling coefficients. The CBM equations provide the evolution of the electric field from the input ($z = z_i$) to the output ($z = z_i + \mathrm{N}a$) of the perturbed section with N unit cells of a LDWG. In

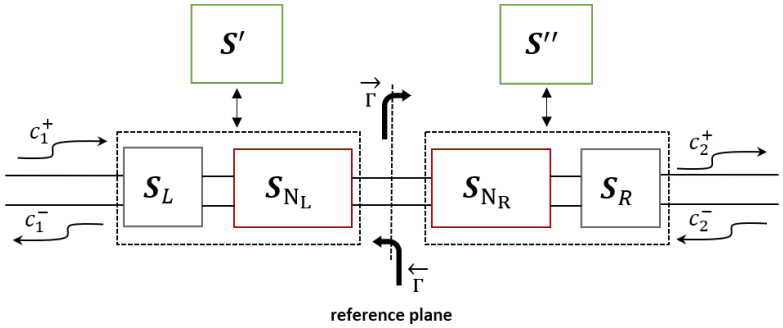

Figure 2: General scheme to compute the complex loop-gain of a LN cavity. The reference plane is put at the interface between two unit cells. $\mathbf{S}_{\mathrm{N}_L}$ ($\mathbf{S}_{\mathrm{N}_R}$) is the scattering matrix of the waveguide located on the left (right), with N_L (N_R) unit cells. The left (right) mirror is described by the scattering matrix $\mathbf{S}_L$ ($\mathbf{S}_R$).

the formulation of Eq. (2.1) and Eq. (2.2), z_i is implicitly set to zero. The amplitudes $c^\pm(z,\omega) = \psi_\pm(z,\omega)e^{\pm ik_z(\omega)z}$

at the input (i) and output (o) of the perturbed section are related through a scattering matrix

$$\begin{bmatrix} c_i^-(\omega) \\ c_o^+(\omega) \end{bmatrix} = \mathbf{S}_{\mathrm{N}}(\omega) \begin{bmatrix} c_i^+(\omega) \\ c_o^-(\omega) \end{bmatrix} \tag{2.3}$$

whose general expression is reported in.[10] The resonance condition of a given longitudinal mode is found by computing the complex loop-gain (LG) of the cavity, as illustrated by Fig. (2). The reference plane to compute the LG is put at the interface between two LDWGs of N_L and N_R unit cells respectively. The cavity is terminated on the left (right) with a mirror modelled by a scattering matrix $\mathbf{S}_L$ ($\mathbf{S}_R$) and the scattering matrix resulting from the cascade of $\mathbf{S}_L$ and $\mathbf{S}_{N_L}$ ($\mathbf{S}_{N_R}$ and $\mathbf{S}_R$) is denoted by $\mathbf{S}'$ ($\mathbf{S}''$). The reflection coefficients at the reference plane are $\overleftarrow{\Gamma} = \mathbf{S}'_{22}$ and $\overrightarrow{\Gamma} = \mathbf{S}''_{11}$ and the LG is $\mathrm{LG} = \overleftarrow{\Gamma} \cdot \overrightarrow{\Gamma}$. If the cavity is passive, the Bloch modes are only coupled at the mirrors, with no distributed coupling. In this case, the self- and cross-coupling coefficients are zero and $\mathbf{S}_{\mathrm{N}}$ reduces to

$$\mathbf{S}_{\mathrm{N}} = \begin{bmatrix} 0 & -e^{-i\delta(\omega)L_{\mathrm{N}}} \\ -e^{-i\delta(\omega)L_{\mathrm{N}}} & 0 \end{bmatrix} \tag{2.4}$$

where $L_{\mathrm{N}} = \mathrm{N}\,a$. This implies $\overleftarrow{\Gamma} = \mathbf{S}_{L,22}\, e^{-2i\delta(\omega)L_{\mathrm{N}_L}}$ and $\overrightarrow{\Gamma} = \mathbf{S}_{R,11}\, e^{-2i\delta(\omega)L_{\mathrm{N}_R}}$, where $L_{\mathrm{N}_L} = \mathrm{N}_L\, a$ and $L_{\mathrm{N}_R} = \mathrm{N}_R\, a$. By assuming $\angle\mathbf{S}_{L,22} = \angle\mathbf{S}_{R,11} = 0$ and denoting by L the cavity length $L_{\mathrm{N}_L} + L_{\mathrm{N}_R}$, the resonance condition $\angle\mathrm{LG} = n2\pi$ for the $n-$th longitudinal mode becomes

$$k_2 - \frac{\pi}{a} = n\frac{\pi}{L} \tag{2.5}$$

where we have denoted k_z by k_2. Eq. (2.5) is the resonance condition reported in.[9] The fundamental resonant mode is obtained for $n = 1$ and is that with the lowest frequency. Since we model a LN cavity as made up of N unit cells (see Fig. (1)), Eq. (2.5) can be recast as

$$\frac{k_2 a}{2\pi} = \frac{1}{2} + \frac{n}{2\mathrm{N}} \tag{2.6}$$

3. BLOCH MODES

We consider LN cavities with air cladding similar to those in.[11] The forward-propogating TE-like Bloch modes $\mathbf{e}_0^+(\mathbf{r})$ of the LDWG on which the LN cavity is based are computed by the plane wave eigensolver MIT Photonic-Bands (MPB).[12] The backward-propagating modes $\mathbf{e}_0^-(\mathbf{r})$ are obtained as the complex conjugate. We denote the x-component of $\mathbf{e}_0^+(\mathbf{r})$ at the middle of the PhC slab ($x = y = 0$) by $e_x^+(z)$. Fig. (3) shows $e_x^+(z)$ in magnitude (a) and phase (b), with each colour corresponding to a different k_z. As an example, each k_z has been chosen as that of the $n-$th resonant mode of a L11 cavity, with $n = 1$ (blue), $n = 2$ (red) and $n = 3$ (yellow). To understand the distribution of the electric field within a LN cavity, we focus on the Fourier harmonics of the Bloch modes $e_x^+(z)$, which we denote by b_q. Fig. (3c) shows them in magnitude at the same frequencies as Fig. (3a) and Fig. (3b). Two important features can be noticed. Firstly, since the phase of $e_x^+(z)$ within a unit cell is almost linear with z, $|b_q|$ is negligigle for $q \neq \{0, -1\}$. Therefore, we can write $e_x^+(z)$ and $e_x^-(z)$ as

$$\begin{aligned} e_x^+(z) &= b_0 + b_{-1} e^{-i\frac{2\pi}{a}z} \\ e_x^-(z) &= \left[e_x^+(z)\right]^\star = b_0^\star + b_{-1}^\star e^{+i\frac{2\pi}{a}z} \end{aligned} \tag{3.1}$$

Secondly, the ratio $|b_{-1}/b_0|$ changes with frequency. This is highlighted by Fig. (3d), which shows $|b_{-1}/b_0|$ versus k_z. The closer to the band edge k_z is and the larger the ratio becomes, because the peak-to-peak amplitude of $e_x^+(z)$ increases. Both the first and second are general features of the Bloch modes of a periodic structure[13] and have a key role in determining if the resonant mode is either FP-like or DFB-like, as it will be clarified in Sec. (5).

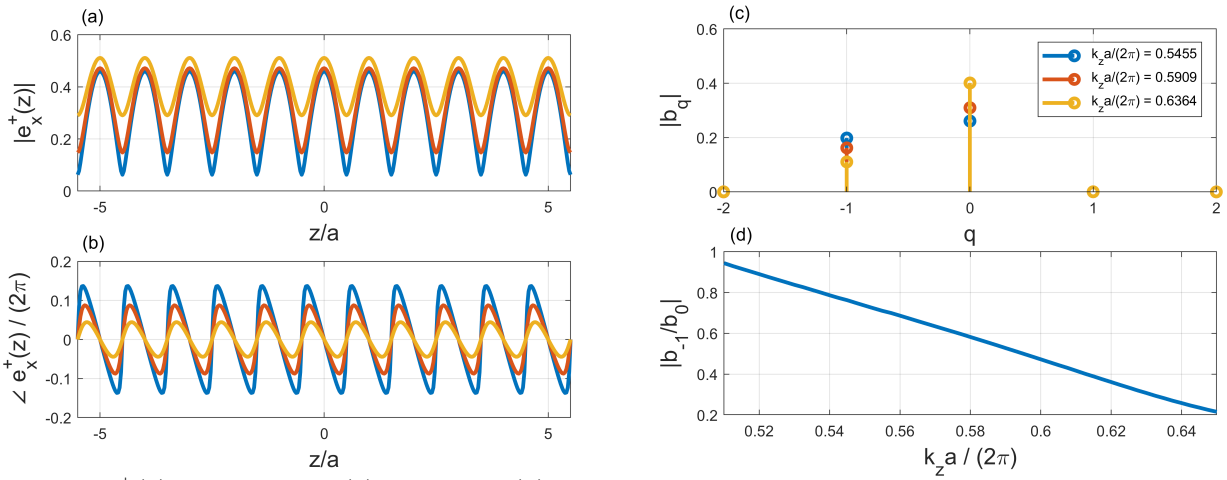

Figure 3: $e_x^+(z)$ in magnitude (a) and phase (b) and magnitude of the corresponding Fourier harmonics b_q (c). Each colour corresponds to the $n-$ th resonant mode of a L11 cavity, with $n = 1$ (blue), $n = 2$ (red) and $n = 3$ (yellow). (d) Magnitude of the ratio between b_{-1} and b_0 as a function of k_z. The Bloch modes have been computed by MPB for an infitinely extended LDWG with air cladding and are normalized such that, at each frequency, the time-averaged energy associated with the electric field $\mathbf{e}_0^+(\mathbf{r})$ is unitary. The lattice constant is 438 nm and the thickness of the slab 250 nm, while the slab refractive index is assumed to be 3.17. The choice of the unit cell is indicated in Fig. (1).

4. RESONANT MODES: REAL-SPACE DISTRIBUTION

We denote by $E_x(z)$ the x-component of the total electric field within the cavity at the middle of the PhC slab. For simplicity, in our analysis we ignore the other in-plane component of the field (z-), as the radiation loss is mainly caused by the x-component.[9] Fig. (4) shows the z-axis, with the centre of the cavity put at $z = 0$. The reference plane of Fig. (2) is put at $z = z_0$, at the interface between two unit cells. In addition, we assume that an integer number of periods of $e_x^+(z)$ fits into the cavity. With these assumptions, at $z = 0$ the magnitude of $e_x^+(z)$ has a maximum (minimum) if N is odd (even). As a consequence, b_0 and b_{-1} are both real and positive if N is odd. If N is even, b_0 is real and positive, while b_{-1} is real and negative.

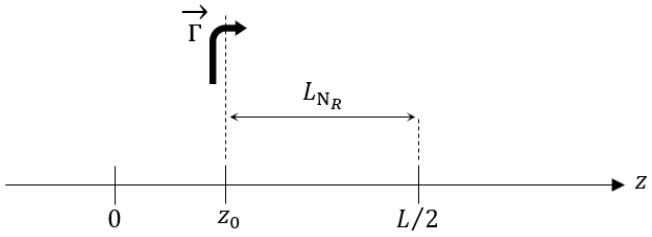

Figure 4: The z axis employed in this paper. The centre of the cavity is at $z = 0$. The reference plane of Fig. (2) is at $z = z_0$, at the interface between two unit cells.

To derive an expression for $E_x(z)$, we need to determine the boundary conditions for the amplitudes $\psi_\pm$. Since there is no distributed coupling, $\psi_\pm$ are constant within the cavity. In practice, the field in the cavity is excited by either optical or electrical pumping. Moreover, since the mirrors are highly-reflective, the output power is collected in the vertical (y-) direction. However, for the sake of simplicity, we assume that the field is excited from the outside at one of the two ends of the cavity. With reference to Fig. (2), we assume an impinging c_1^+,

while $c_2^- = 0$. Therefore, $c^{\pm}(z)$ at the reference plane are given by

$$\begin{aligned} c^+(z_0) &= c_1^+ \frac{\mathbf{S}'_{21}}{1 - LG} \\ c^-(z_0) &= c^+(z_0)\overrightarrow{\Gamma} \end{aligned} \tag{4.1}$$

The amplitudes $c^{\pm}(z)$ in the other points are given by $c^{\pm}(z) = \psi_{\pm} e^{\pm i k_2 (z - z_0)}$. Therefore, we can compute ψ^+ and ψ^- as

$$\begin{aligned} \psi_+ &= c_1^+ \frac{\mathbf{S}'_{21}}{1 - LG} \\ \psi_- &= \psi^+ \overrightarrow{\Gamma} \end{aligned} \tag{4.2}$$

The phase of ψ_+ can be related to the phase of $c^+(z)$ at the centre of the cavity by

$$\angle \psi^+ = k_2 z_0 + \phi \tag{4.3}$$

with $\phi = \angle c^+(z = 0)$, while from Eq. (4.2) the phase of ψ^- is obtained as

$$\angle \psi^- = \angle \psi^+ + \angle \overrightarrow{\Gamma} \tag{4.4}$$

A mode propagating within a LN cavity is confined within it because it is evanescent within the mirrors.[14] For simplicity, we model the mirrors as concentrated and frequency-independent. Within this approximation, the evanescent decay of the field within the mirrors cannot be reproduced and the field distribution can only be recovered within the cavity, where the electric field can be approximately written as

$$E_x(z) = w(z, L) \left[\psi^+ e_x^+(z) e^{+ i k_2 (z - z_0)} + \psi^- e_x^-(z) e^{- i k_2 (z - z_0)} \right] \tag{4.5}$$

Here, the window function $w(z, L)$ accounts for the field confinement provided by the mirrors and is defined as

$$w(z, L) = \begin{cases} 1, & |z| \leq L/2 \\ 0, & |z| > L/2 \end{cases} \tag{4.6}$$

The input and output plane of the cavity are put at $z = -L/2$ and $z = L/2$ respectively, as indicated in Fig. (1). Since $|\overrightarrow{\Gamma}| = |\mathbf{S}_{R,11}|$, then $|\psi_+| = |\psi_-|$ if the right mirror reflectivity is unitary. For simplicity, we will assume in the following $|\mathbf{S}_{R,11}| = 1$. Therefore, by taking into account that b_0 and b_{-1} are both real and plugging Eq. (3.1) into Eq. (4.5), we obtain

$$\begin{aligned} E_x(z) = w(z, L) \Big[& |\psi^+| \left(b_0 + b_{-1} e^{-i \frac{2\pi}{a} z} \right) e^{+ i k_2 (z - z_0)} e^{+ i \angle \psi_+} \\ & + |\psi^+| \left(b_0 + b_{-1} e^{+i \frac{2\pi}{a} z} \right) e^{- i k_2 (z - z_0)} e^{+ i \angle \psi_-} \Big] \end{aligned} \tag{4.7}$$

Furthermore, consistently with,[9] we define

$$k_1 = \frac{2\pi}{a} - k_2 \tag{4.8}$$

4.1 LN cavity with N odd

If N is odd, z_0 is given by $z_0 = \pm \left(m + \frac{1}{2}\right) a$, with m being an integer. By exploiting Eq. (2.5) and writing L_{N_R} as $L_{\mathrm{N}_R} = L/2 - z_0$ (see Fig. (4)), we can express the phase of $\overrightarrow{\Gamma}$ at the n-th resonance as

$$\angle \overrightarrow{\Gamma} = (n \pm 1)\pi - 2 k_2 z_0 \tag{4.9}$$

This implies $\angle \psi_- = -k_2 z_0 + (n \pm 1)\pi + \phi$. Therefore, the electric field distribution $E_x(z)$ is obtained from Eq. (4.7) as

$$\begin{aligned} E_x(z) = w(z, L) e^{+ i \phi} \Big[& |\psi^+| b_0 e^{+ i k_2 z} + |\psi^+| b_{-1} e^{- i k_1 z} \\ & + |\psi^+| b_0 e^{- i k_2 z} e^{+ i (n \pm 1)\pi} + |\psi^+| b_{-1} e^{+ i k_1 z} e^{+ i (n \pm 1)\pi} \Big] \end{aligned} \tag{4.10}$$

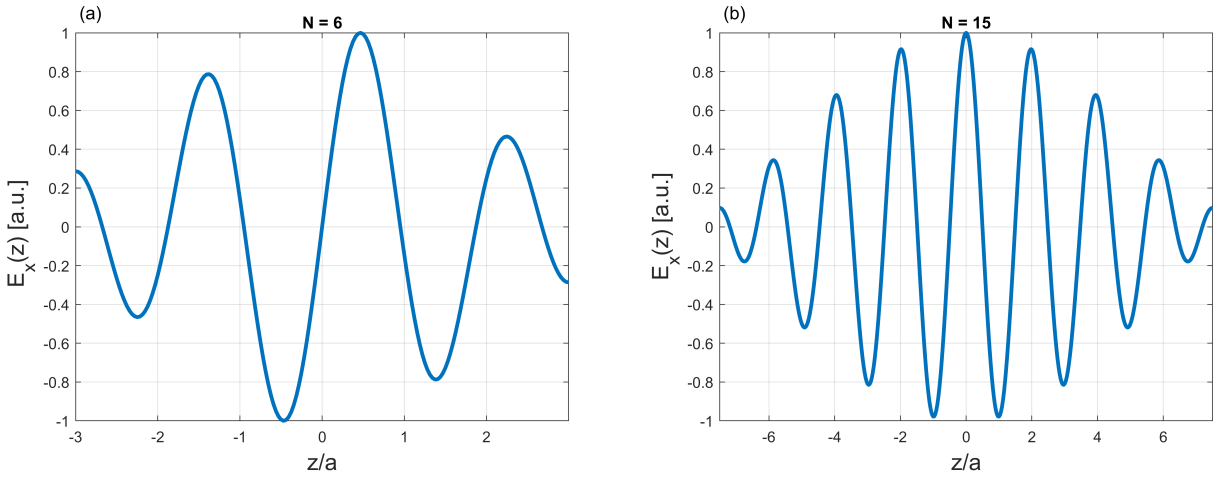

Figure 5: (a) Fundamental mode real-space distribution in a L6 cavity computed by Eq. (5.1). (b) Fundamental mode real-space distribution in a L15 cavity computed by Eq. (5.2). The input and output plane of the cavity are those indicated in Fig. (1). Reproducing the evanescent decay of the field within the mirrors is beyond the scope of this paper.

Since b_0 and b_{-1} are both real and positive, Eq. (4.10) can be recast as

$$\begin{aligned} E_x(z) &= w(z,L)\, 2|\psi_+|e^{+i\phi}\left[|b_0|\cos(k_2 z) + |b_{-1}|\cos(k_1 z)\right], \quad \text{for } n \textbf{ odd} \\ E_x(z) &= w(z,L)\, 2i|\psi_+|e^{+i\phi}\left[|b_0|\sin(k_2 z) + |b_{-1}|\sin(k_1 z)\right], \quad \text{for } n \textbf{ even} \end{aligned} \tag{4.11}$$

Consistently with,[9] $E_x(z)$ is even (odd) with respect to the centre of the cavity if n is odd (even).

4.2 LN cavity with N even

If N is even, then $z_0 = \pm ma$, with m being an integer. The phase of $\overrightarrow{\Gamma}$ can be written as

$$\angle\overrightarrow{\Gamma} = n\pi - 2k_2 z_0 \tag{4.12}$$

from which $\angle\psi_- = -k_2 z_0 + n\pi + \phi$. Consequently, from Eq. (4.7) $E_x(z)$ can be written as

$$\begin{aligned} E_x(z) = w(z,L)e^{+i\phi}\big[&|\psi^+|b_0 e^{+ik_2 z} + |\psi^+|b_{-1}e^{-ik_1 z} \\ &+ |\psi^+|b_0 e^{-ik_2 z}e^{+in\pi} + |\psi^+|b_{-1}e^{+ik_1 z}e^{+in\pi}\big] \end{aligned} \tag{4.13}$$

Since b_0 is real and positive, while b_{-1} is real and negative, Eq. (4.13) can be rearranged as

$$\begin{aligned} E_x(z) &= w(z,L)\, 2i|\psi_+|e^{+i\phi}\left[|b_0|\sin(k_2 z) + |b_{-1}|\sin(k_1 z)\right], \quad \text{for } n \textbf{ odd} \\ E_x(z) &= w(z,L)\, 2|\psi_+|e^{+i\phi}\left[|b_0|\cos(k_2 z) - |b_{-1}|\cos(k_1 z)\right], \quad \text{for } n \textbf{ even} \end{aligned} \tag{4.14}$$

In agreement with,[9] $E_x(z)$ is odd (even) with respect to centre of the cavity if n is odd (even).

5. FUNDAMENTAL MODE

We focus now on the real-space and wavevector-space distribution of the fundamental mode. Based on the results of Sec. (4), the analysis can be easily extended to higher-order longitudinal modes. If N is odd and $n = 1$, from Eq. (4.11) $E_x(z)$ is given by

$$\begin{aligned} E_x(z) = w(z,L)|\psi_+|\big[&|b_0|e^{+ik_2 z} + |b_0|e^{-ik_2 z} \\ &+ |b_{-1}|e^{+ik_1 z} + |b_{-1}|e^{-ik_1 z}\big], \quad \text{for N } \textbf{odd} \end{aligned} \tag{5.1}$$

where we have put $\phi = 0$. If N is even and $n = 1$, from Eq. (4.14) we obtain

$$E_x(z) = -w(z,L)i|\psi_+|\left[|b_0|e^{+ik_2 z} - |b_0|e^{-ik_2 z} + |b_{-1}|e^{+ik_1 z} - |b_{-1}|e^{-ik_1 z}\right], \quad \text{for N } \textbf{even} \tag{5.2}$$

where we have put $\phi = -\pi/2$. As an example, the fundamental mode is shown in Fig. (5a) for N = 6 and in Fig. (5b) for N = 15. Independently if N is either odd or even, the real-space distribution of $E_x(z)$ results from the superimposition of two pairs of plane waves, with wavevectors $\pm k_1$ and $\pm k_2$. The ratio $|b_{-1}/b_0|$ between the amplitudes of these plane waves is the ratio between the Fourier harmonics of either of the two Bloch modes circulating within the cavity. As N varies, the resonance frequency changes and the ratio $|b_{-1}/b_0|$ correspondingly varies. This is outlined by Fig. (6), which displays k_2 and $|b_{-1}/b_0|$ versus N. From (2.6) and (4.8), the wavevector k_1 can be also expressed as

$$\frac{k_1 a}{2\pi} = \frac{1}{2} - \frac{1}{2\mathrm{N}} \tag{5.3}$$

where we have put $n = 1$. As N increases, both k_1 and k_2 move towards the band edge. Therefore, as

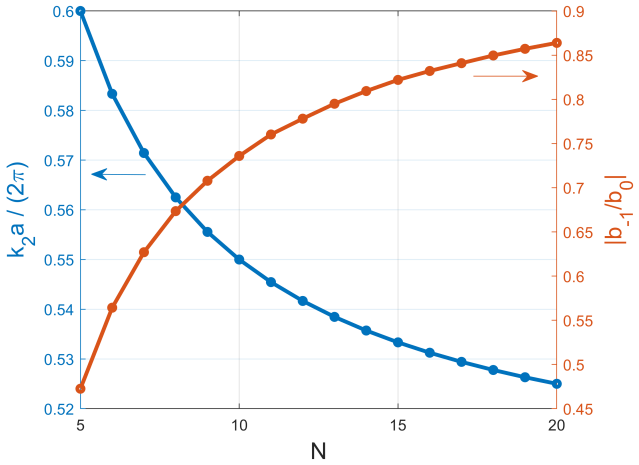

Figure 6: k_2 as determined by the resonance condition (left) and corresponding $|b_{-1}/b_0|$ (right) versus N.

outlined in Sec. (3), $|b_{-1}|$ gradually becomes comparable to $|b_0|$ and the fundamental mode tends to become DFB-like according to the nomenclature proposed in.[9] This nomenclature originates from the fact that the field distribution in a DFB laser is determined by two pairs of wavevectors, namely $\pm k_1$ and $\pm k_2$.[15] On the contrary, the smaller N is and the more $E_x(z)$ is determined by a single pair of plane waves, with wavevectors $\pm k_2$, as it occurs in a FP laser. For this reason, the fundamental mode turns into FP-like. Eq. (5.1) and Eq. (5.2) coincide with those reported in[9] for the fundamental mode. However, these expressions are therein obtained through a fitting procedure with FDTD simulations. As compared to,[9] here we have shown that the expression for $E_x(z)$ naturally follows from the expansion of the field in the two counter-propagating Bloch modes of the cavity. In addition, we have highlighted the physical meaning of b_{-1} and b_0, as well as the origin for the dependence of $|b_{-1}/b_0|$ on the size of the cavity. Having shed light on the real-space profile of the fundamental mode, we focus now on its distribution in the wavevector-space. From Eq. (5.1) and Eq. (5.2), we compute the spatial Fourier transform of $E_x(z)$ as

$$E_x(\zeta) = |\psi_+|\left[|b_0|W(\zeta - k_2) + |b_0|W(\zeta + k_2) + |b_{-1}|W(\zeta - k_1) + |b_{-1}|W(\zeta + k_1)\right], \quad \text{for N } \textbf{odd} \tag{5.4}$$

$$E_x(\zeta) = -i|\psi_+|\left[|b_0|W(\zeta - k_2) - |b_0|W(\zeta + k_2) + |b_{-1}|W(\zeta - k_1) - |b_{-1}|W(\zeta + k_1)\right], \quad \text{for N } \textbf{even} \tag{5.5}$$

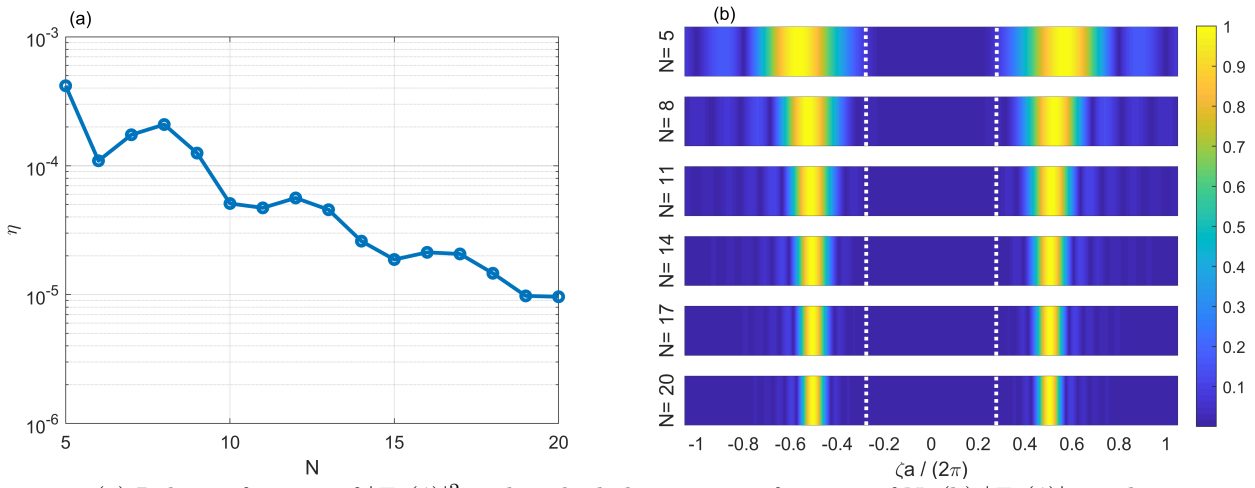

Figure 7: (a) Relative fraction of $|E_x(\zeta)|^2$ within the light cone as a function of N. (b) $|E_x(\zeta)|$ in arbitrary units for the fundamental mode of LN cavities with different values of N. For each N, the white, dotted lines delimit the light cone.

where ζ is the spatial angular frequency and $W(\zeta)$ is the spatial Fourier transform of $w(z, L)$

$$W(\zeta) = L\frac{\sin(\zeta L/2)}{\zeta L/2} = L\text{sinc}\left(\frac{\zeta L}{2\pi}\right) \tag{5.6}$$

For a given N, the wavevector components of the field fullfilling the condition $|\zeta| > (\omega_2/c)\, n_{\text{clad}}$ are confined to the slab in the vertical direction by total internal reflection. Here, n_{clad} is the cladding refractive index (in our case, $n_{\text{clad}} = 1$) and ω_2 is the angular frequency of the longitudinal mode. The other ζ components lie in the light cone and couple to the continuum of radiative modes. As a measure of the scaling of the radiation loss with the size of the cavity, we report in Fig. (7a) the relative fraction of the electric field intensity within the light cone

$$\eta = \frac{\int_{-\zeta_0}^{+\zeta_0} |E_x(\zeta)|^2 d\zeta}{\int_{-\infty}^{+\infty} |E_x(\zeta)|^2 d\zeta} \tag{5.7}$$

where $\zeta_0 = \omega_2/c$ is the upper limit of the light cone for a given N. The scaling is compatible with that reported in[11] for LN cavities without disorder and confirms that the radiation loss significantly decreases as the cavity becomes longer. As N increases, k_1 tends to π/a and $W(\zeta \pm k_1)$ departs from the light cone. In addition, the spectral width of each of the sinc functions in Eq. (5.4) and Eq. (5.5) decreases as the cavity becomes longer. This is evidenced by Fig. (7b), showing $|E_x(\zeta)|$ for different values of N. As a result, the mode spectrum shifts outside the light cone and the relative fraction η decreases.

6. CONCLUSIONS

By applying the coupled-Bloch-mode approach presented in,[10] we have derived the resonance condition for the n-th longitudinal mode of a passive PhC line-defect cavity with N missing holes (a so called LN cavity) and simple expressions for the electric field within it. We have outlined that the symmetry of the electric field with respect to the centre of the cavity depends both on n and N and is consistent with that reported in.[9] We have then focused on then fundamental mode and shown that, as N increases, it turns from FP-like to DFB-like according to the nomenclature proposed in.[9] As compared to,[9] we have clarified the physical origin for this behaviour and traced it back to the Fourier harmonics of the Bloch modes circulating within the cavity. Finally, we have analyzed the fundamental mode distribution in the wavevector-space. Consistently with,[11] we have shown that the relative fraction of the mode spectrum within the light cone is gradually suppresed as N increases. In conclusion, we believe that the investigation illustrated in this paper will contribute to a more fundamental understanding of the characteristics of PhC cavities and might provide useful insights for their design.

REFERENCES

[1] Matsuo, S. and Kakitsuka, T., "Low-operating-energy directly modulated lasers for short-distance optical interconnects," *Adv. Opt. Photon.* **10**, 567–643 (Sep 2018).

[2] Takeda, K., Sato, T., Shinya, A., Nozaki, K., Kobayashi, W., Taniyama, H., Notomi, M., Hasebe, K., Kakitsuka, T., and Matsuo, S., "Few-fj/bit data transmissions using directly modulated lambda-scale embedded active region photonic-crystal lasers," *Nature Photonics* **7**(7), 569–575 (2013).

[3] Fitsios, D. and Raineri, F., "Chapter five - photonic crystal lasers and nanolasers on silicon," in [*Silicon Photonics*], Lourdudoss, S., Chen, R. T., and Jagadish, C., eds., *Semiconductors and Semimetals* **99**, 97 – 137, Elsevier (2018).

[4] Mork, J., Chen, Y., and Heuck, M., "Photonic crystal fano laser: Terahertz modulation and ultrashort pulse generation," *Phys. Rev. Lett.* **113**, 163901 (Oct 2014).

[5] Yu, Y., Xue, W., Semenova, E., Yvind, K., and Mørk, J., "Demonstration of a self-pulsing photonic crystal fano laser," *Nature Photonics* **11**(2), 81–84 (2017).

[6] Rasmussen, T. S., Yu, Y., and Mork, J., "Suppression of coherence collapse in semiconductor fano lasers," *Phys. Rev. Lett.* **123**, 233904 (Dec 2019).

[7] Vuckovic, J., Loncar, M., Mabuchi, H., and Scherer, A., "Optimization of the Q factor in photonic crystal microcavities," *IEEE Journal of Quantum Electronics* **38**, 850–856 (July 2002).

[8] Asano, T., Song, B., Akahane, Y., and Noda, S., "Ultrahigh-Q nanocavities in two-dimensional photonic crystal slabs," *IEEE Journal of Selected Topics in Quantum Electronics* **12**, 1123–1134 (Nov 2006).

[9] Okano, M., Yamada, T., Sugisaka, J., Yamamoto, N., Itoh, M., Sugaya, T., Komori, K., and Mori, M., "Analysis of two-dimensional photonic crystal L-type cavities with low-refractive-index material cladding," *Journal of Optics* **12**, 075101 (jun 2010).

[10] Saldutti, M., Bardella, P., Mørk, J., and Gioannini, M., "A Simple Coupled-Bloch-Mode Approach to Study Active Photonic Crystal Waveguides and Lasers," *IEEE Journal of Selected Topics in Quantum Electronics* **25**, 1–11 (Nov 2019).

[11] Xue, W., Yu, Y., Ottaviano, L., Chen, Y., Semenova, E., Yvind, K., and Mork, J., "Threshold characteristics of slow-light photonic crystal lasers," *Phys. Rev. Lett.* **116**, 063901 (Feb 2016).

[12] Johnson, S. G. and Joannopoulos, J. D., "Block-iterative frequency-domain methods for Maxwell's equations in a planewave basis," *Opt. Express* **8**, 173–190 (Jan 2001).

[13] Yu, T., Wang, L., and He, J.-J., "Bloch wave formalism of photon lifetime in distributed feedback lasers," *J. Opt. Soc. Am. B* **26**, 1780–1788 (Sep 2009).

[14] Joannopoulos, J. D., Johnson, S. G., Winn, J. N., and Meade, R. D., [*Photonic Crystals: Molding the Flow of Light (Second Edition)*], Princeton University Press, 2 ed. (2008).

[15] Coldren, L. A., Corzine, S. W., and Mašanović, M. L., [*Diode Lasers and Photonic Integrated Circuits*], John Wiley & Sons (2012).